Permeability Prediction from Thin Sections using the Lattice-Boltzmann Flow Simulation

Youngseuk Keehm, Tapan Mukerji, Manika Prasad and Amos Nur*
Rock Physics Laboratory, Geophysics Department, Stanford University, CA 94305.

Summary

This paper presents a new methodology for predicting permeability from thin sections. The method is based on two key components – constructing 3D porous media from 2D thin sections and a direct 3D flow simulation using the Lattice-Boltzmann (LB) method. From a thin section, statistical parameters such as porosity and autocorrelation function are calculated through image processing. We construct 3D porous media using a geostatistical method of sequential indicator simulation conditioned to the thin section. We then perform flow simulations on those 3D realizations without idealizing or simplifying the complex pore geometry. The LB flow simulation method can successfully handle realistic and very complicated 3D pore geometries. We apply our method for seven thin sections from Daqing oil field. Predicted permeabilities show excellent agreement with lab measurements. We then compare our method to another one, which also estimates permeability based on statistical parameters from thin sections, but without flow simulation. Our method gives better results and is less sensitive to statistical noise from image processing of thin sections. More importantly, our method does not require any empirical parameters.

Introduction

The prediction of permeability remains one of the most important challenges in quantitative rock physics. Many relatively successful and common methods are empirical ones, such as the Kozeny-Carman relation based on simple cylindrical pore geometry. These models have been widely applied because they are easy to use and are simple to understand (Dullien, 1992; Mavko and Nur, 1997). Walsh and Brace (1984) used a variant of the Kozeny-Carman relation, which relates the permeability to porosity, a geometrical factor, the formation factor and the specific surface area. They applied the relationship for low porosity and low permeability granites. However, most of these parameters are not easy to measure from samples or thin sections, especially, the specific surface area. Blair et al. (1993) chose a very similar approach, but they calculated the specific surface area of thin sections by a formula by Berryman (1987). Estimated permeability agreed well with lab measurement. However, the calculation of the specific surface area from images is sensitive to the resolution of thin section images. A small change in image resolution gives a relatively large error in estimated permeability. In addition, empirical estimates or laboratory measurements are still required for geometrical parameter and formation factor. Adler et al. (1990) chose a different approach. They measured porosity and autocorrelation function from binary thin sections and generated 3D structures based on the unconditional truncated Gaussian method. One slight complication comes in at the estimation of the correlation function from the binary thin section, since the correlation of the binary image is not the same as that of the Gaussian random function. They then applied an alternating-direction-implicit finite difference scheme on the simulated 3D porous media to solve Stokes flow of a Newtonian fluid. Estimated permeabilities for five Fontainebleau sandstone samples agreed reasonably well with lab measurements. However, the size of simulated cubes does not seem to be big enough to represent fluid flow of the whole rock, and the LB can be more accurate that the FDM for complex media (Sangani and Acrivos, 1982; Ladd 1994). Liang et al. (1999) suggested a similar Gaussian truncation method to generate 3D porous media from thin sections. However, they processed simulated 3D pore geometry further into skeletons by a thinning algorithm that can preserve connectivity. They then perform network modeling from the skeleton to estimate permeability. Even though they start with the full 3D pore geometry, they ultimately simplify it into a network, which means arbitrarily altering the pore structure.

Our method also uses a technique based on binary images of thin sections. However, rather than resorting to an empirical relation or network modeling, we generate realizations of 3D porous media by conditional sequential indicator simulation with statistical parameters from the 2D binary image. Since we deal with binary 3D porous media, an algorithm based on a binary indicator function is more natural and straightforward than the continuous Gaussian function. After obtaining multiple stochastic realizations, we perform fluid flow simulations using the Lattice-Boltzmann method on the simulated 3D pore geometries. The Lattice-Boltzmann method is robust enough to handle very complicated simulated 3D structures with statistical noise. Seven different thin section samples from the Daqing oil field were used for this study (Prasad and Nur, submitted). We also compare our method to the one by Blair et al. (1993). In the following sections, we will cover details of methodology and results with our sandstones samples. Finally, comparison to another conventional method will follow.

Thin Section Data and Image Processing

Thin sections were obtained from sandstone samples from Daqing oil field. They are relatively clean sandstones with clay content between 4-10%. Porosity and Klinkenberg-corrected air permeability were measured at room pressure and at 5.5 MPa confining pressure under controlled room

temperature. The porosity varies from 20% to 30% and the range of the permeability is 40mD to 1,700mD (Table 1).

Table 1: Porosity and permeability from laboratory measurement and from the flow simulation on reconstructed 3D porous media.

Sample#	Porosity (%)		Permeability (mD)	
	Lab	Estimated	Lab	Estimated
1	30.0	28.7	1,766	1,679
2	26.9	27.8	1,030	1,431
3	25.2	25.6	818	946
4	28.1	29.0	591	566
5	23.4	24.7	295	320
6	22.0	20.8	91	101
7	20.1	20.0	39	61

Since the sandstone samples were saturated by epoxy, the pore space is clearly distinguishable (Figure 1). Blue color denotes pores and others are grains. The image consists of 600×400 pixels and yellow scale bars denotes 1mm. From the color image of the thin section, a binary image can be obtained using simple image processing. We converted the true color image into an index image, and selected proper indices for grains and pore space. Then, the binary image can be represented by an indicator function $f(r)$,

$$f(r) = \begin{cases} 1 & \text{if } r \text{ belongs to pore space,} \\ 0 & \text{otherwise,} \end{cases} \quad (1)$$

where r denotes a spatial location within the binary image.

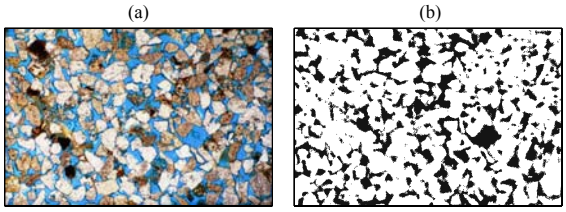

Figure 1: (a) Scanned image from an epoxy-saturated thin section. Blue color denotes pores and the yellow bar is 1mm. (b) Binary image after image processing. The pore space appears in black.

The porosity ϕ and the autocorrelation function $A(\mathbf{h})$, (i.e. the two-point correlation function) can be defined by the statistical averages, denoted by <·>,

$$\phi = < f(r) >, \quad A(\mathbf{h}) = < f(r) f(r+\mathbf{h}) > \quad (2)$$

where $\mathbf{h}$ is a lag vector between two data points. Two important properties of the autocorrelation function of the binary image are (Blair et al., 1993)

$$A(0) = \phi, \quad \lim_{|\mathbf{h}|\to\infty} A(\mathbf{h}) = \phi^2 . \quad (3)$$

The autocorrelation function can be easily obtained using Fourier transforms,

$$A(\mathbf{h}) = F^{-1}\{ F\{f(r)\} \cdot F^{*}\{f(r)\} \} \quad (4)$$

where $F\{\cdot\}$ and $F^{-1}\{\cdot\}$ denote 2D Fourier and inverse Fourier transforms, and * denotes the complex conjugate. Figure 2 shows a 2D autocorrelation function of the binary image from Figure 1. Two orthogonal 1D autocorrelation functions (horizontal and vertical) in Figure 2(b) indicate that the binary image is fairly isotropic since the difference is negligible. The autocorrelation length a is closely related to the characteristic pore scale. The porosity measured from the binary image is 0.29. We can see that Equation 3 is successfully verified in Figure 2(b).

To calculate meaningful statistical parameters from thin section images, we need much larger image size (L) than the correlation length, as shown in Figure 3. Squares of different sizes were chosen from the binary image for the calculation of the statistical parameters. When L/a is very small, porosity fluctuates. It however, converges to the lab measurement when L/a>10. The autocorrelation functions in Figure 3(c) also show very similar behavior to that of porosity. When L>10a, we can safely assume that it is a representative elementary area. We used thin section images larger than 20a for accurate estimation of statistical parameters. We also found that all our samples are fairly isotropic, which means that we can now assume that the 2D parameters are valid for 3D rocks. All porosities from thin sections show good agreement with lab measurements and the differences are less than 2% (Table 1).

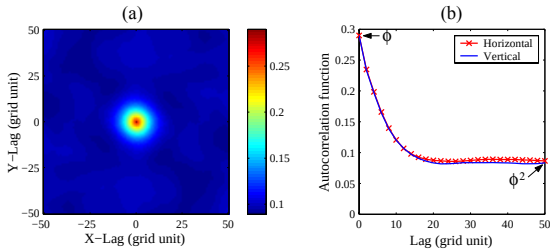

Figure 2: (a) 2D autocorrelation function from the binary image. (b) Horizontal and vertical autocorrelation functions (1D) and autocorrelation length (a).

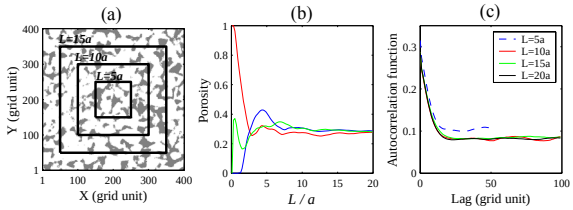

Figure 3: (a) Different square for estimating statistical parameters. (b) Porosity given by different sized squares. (c) Autocorrelation functions, $A(h)$. When L≥10a, $A(h)$ and ϕ from different sized squares are very close to each other.

2D to 3D Porous Media by Stochastic Simulation

To simulate stochastic realizations of 3D porous media, we used a geostatistical approach (Deutsch and Journel, 1998). We first performed variogram modeling. The variogram has nearly the same meaning as the autocorrelation function, except that it reflects the dissimilarity of data in

spatial distribution instead of similarity. The variogram can be related to the autocorrelation function,

$$\gamma(\mathbf{h}) = \frac{1}{2n(\mathbf{h})}\sum_{i=1}^{n(\mathbf{h})}\{f(r_i) - f(r_i+\mathbf{h})\}^2 = A(0) - A(\mathbf{h}) \quad (5)$$

where $n(\mathbf{h})$ is the number of pairs of data locations with a vector $\mathbf{h}$ apart. This raw experimental variogram is then modeled by an exponential function to ensure positive-definiteness of the variogram model. The exponential variogram is given as follows:

$$\gamma(\mathbf{h}) = c\,\{1 - \exp(-3\mathbf{h}/a)\}\,. \quad (6)$$

Figure 4 shows variograms along different directions and the variogram model. The variogram model is the best fit for raw variograms with a nonlinear least squares fitting by the Gauss-Newton method. Using the variogram model, multiple realizations of 3D porous media were simulated conditioned to the thin section. The algorithm was the sequential indicator simulation (SISim) of the geostatistics software library. Details can be found in Keehm (2003). Figure 5 shows an example of simulated 3D porous media. Since the flow simulation requires a periodic BC along the flow direction, the same conditional data from the thin section image are included at both ends of the cube. We generated no less than 10 different realizations of simulated 3D cubes for each thin section. We then calculated statistical parameters of the simulated 3D porous media to verify that the simulated realization has the same statistical properties. The variograms from the simulated 3D porous media were very close to the variogram model, which means the simulated 3D realization has the same statistical properties as the thin section.

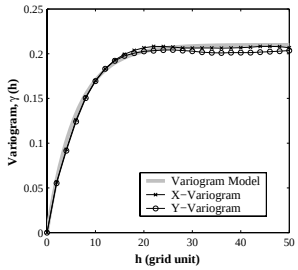

Figure 4: Variogram modeling. Circles denote X-variogram, squares denote Y-variogram, and a solid line is a variogram model.

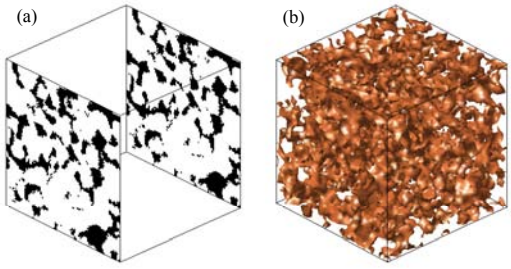

Figure 5: (a) Conditional data for the SISim. (b) Isosurface plot of a 3D realization by the sequential indicator simulation.

Permeability Estimation by the LB Flow Simulation

The stochastically simulated 3D porous media are very complex and may contain statistical noise from the simulation. The Lattice-Boltzmann method for numerical flow simulation can be an excellent choice, since it can handle complex pore geometry without any simplifications (Ladd, 1994; Spaid and Phelan, 1997; Bosl et al., 1998; Keehm et al., 2001). Figure 6 shows the distribution of local fluid flux after the flow simulation. The effective flow paths and their complexity can be clearly seen in cross-sectional plots. The permeability can simply be calculated by Darcy's law. Results from all seven thin sections can be found in Table 1. Porosity and permeability estimations are reasonably consistent with lab measurements. All estimated values reflect very good agreement with lab measurements (Figure 7). The correlation coefficient between estimated permeability and laboratory measurement is 0.96, which implies excellent prediction.

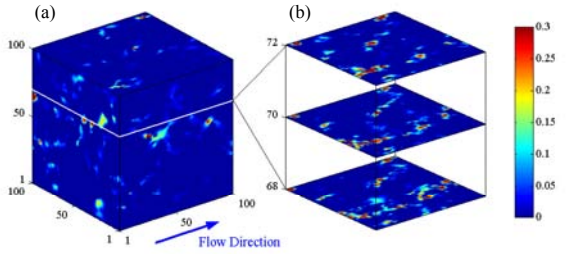

Figure 6: (a) Local mass flux by the Lattice-Boltzmann flow simulation. Flux values are normalized by the maximal value. (b) Cross-sectional plots of the high flux area.

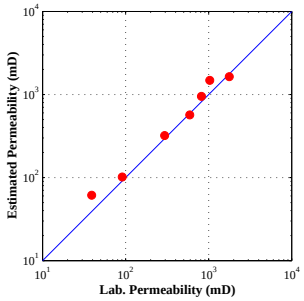

Figure 7: Calculated permeabilities versus lab measurements for all seven samples used in this study.

Comparison to the Method by Blair et al.

Walsh and Brace (1984) derived a similar formula relating permeability to porosity, formation factor (F) and the specific surface area:

$$\kappa = \phi^2/(c\,F^2 S^2) \quad (7)$$

where c is a geometric factor, with c=2 for circular pores and c=3 for flat cracks. This is a variant of Kozeny-Carman relation, where the formation factor replaces the tortuosity,

which is hardly measurable. Blair et al. (1993) suggested that Equation 7 would be useful for estimating permeability from thin sections. To determine the specific surface area, they used a relationship between the specific surface area and the spatial correlation functions (Berryman, 1987),

$$S = -4 \times A'(0) \tag{8}$$

where $A'(0)$ is the slope of the two-point correlation function at the origin. Since $A(\mathbf{h})$ is a discrete function, we need very high-resolution images for accurate calculation of $A'(0)$. In addition, the estimation of the specific surface area is sensitive to the image resolution. Blair et al. (1993) suggested that $a \cong 100d$ as an optimal resolution, where d is grid spacing. However, even a slight change in resolution will significantly change the permeability estimation. In addition, the formation factor (F) and the geometric factor (c) need to be obtained from sources other than the 2D images, such as lab measurements or empirical relations. We applied Blair et al.'s (1993) method to our data set. Figure 8 shows comparison between our method and Blair et al.'s. Both show a reasonably good match, but our method gives better agreement. One interesting observation is that two methods show very similar error trends, which suggests a common error source: the statistical parameters from the thin section image. It appears our method is less sensitive to the statistical errors, because our method does not involve the derivative, which would be sensitive to even a small noise.

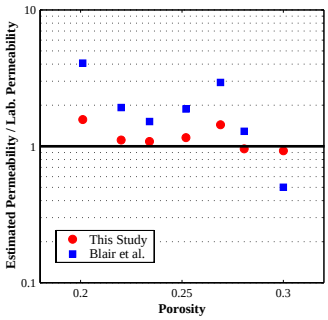

Figure 8: Permeability estimations from the seven thin sections by Blair et al. (squares) and by this study (dots).

Conclusions

The Lattice-Boltzmann flow simulation on stochastically reconstructed 3D porous media is a robust combination for permeability prediction from thin sections. It seems quite remarkable that direct flow simulations on stochastically constructed 3D porous media provide very good agreement with lab measurements over a wide range of permeability. We found that determining the statistical parameters ($A(\mathbf{h})$ and ϕ) should be carefully performed, since all following procedures are strongly dependent on these statistical parameters. For accurate calculation of these parameters and flow simulation, we recommend $L \geq 10a$ and $dx \leq a/10$. The sequential indicator simulation successfully generates multiple realistic 3D porous media. The LB simulation shows its strength in handling these complicated 3D pore geometries. The estimated permeability shows very good agreement with lab measurements. Permeability prediction by Blair et al. (1993) gives good estimates of permeability. However, the estimation of the specific surface area is dependent on image resolution and is very sensitive to changes in resolution. The error in estimation is about 2~3 times higher than our method. Both methods show similar error trends in permeability estimation. This implies that the statistical parameters from the thin section do not fully represent the whole rock. Practically, this cannot be avoidable. The results indicate that our method is less sensitive to the small discrepancy between thin sections and rock samples. In addition, our method does not require any empirical parameters and lab measurements.

References

Adler, P. M., Jacquin, C. G. and Quiblier, J. A., 1990, Flow in simulated porous media, Int. J. Multiphase Flow, 16, 691–712.

Berryman, J. G., 1987, Relationship between specific surface area and spatial correlation functions for anisotropic porous media, J. Math. Phys., 28, 245–246.

Blair, S. C., Berge, P. A., and Berryman, J. G., 1993, Two-point correlation functions to characterize microgeometry and estimate permeabilities of synthetic and natural sandstones, Lawrence Livermore National Laboratory Report, Livermore.

Bosl, W. J., Dvorkin, J., and Nur, A., 1998, A numerical study of pore structure and permeability using a Lattice Boltzmann Simulation, Geophy. Res. Lett., 25, 1475–1478.

Deutsch, C. V., and Journel, A. G., 1998, GSLIB: Geostatical Software Library and User's Guide, Oxford Univ. Press, 369pp.

Dullien, F. A. L., 1992, Porous Media: Fluid Transport and Pore Structure, Academic Press, 574pp.

Keehm, Y., 2003, Computational rock physics: transport properties of porous media and applications, Ph.D. Thesis, Stanford Univ.

Keehm, Y., Mukerji, T., and Nur. A., 2001, Computational rock physics at the pore scale: Transport properties and diagenesis in realistic pore geometries, The Leading Edge, 20, 180–183.

Ladd, A. J. C., 1994, , Numerical simulations of particulate suspensions via a discretized Boltzmann equation: Part 2. Numerical results, J. Fluid. Mech., 271, 311–339.

Liang, Z. R., Ioannidis, M. A. and Chatzis, I., 2000, Permeability and electrical conductivity of porous media from 3D stochastic replicas of the microstructure, Chem. Eng. Sci., 55, 5247–5262.

Mavko, G., and Nur, A., 1997, Effect of a percolation threshold in the Kozeny-Carman relation, Geophysics, 62, 1480–1482.

Prasad, M. and Nur, A., submitted to Geophysics, Acoustic and depositional properties of fluviatile sandstones.

Spaid, M. A. A., and Phelan, F. R., Jr., 1997, Lattice Boltzmann methods for modeling microscale flow in fibrous porous media, Phys. Fluids, 9, 2468–2474.

Walsh, J. B., and Brace, W. F., 1984, The effect of pressure on porosity and transport properties of rock, JGR, 89, 9425–9431.